Nanometer Beam-Size Measurement during Collisions at Linear Colliders *

T. Tauchi and K. Yokoya
National Laboratory for High Energy Physics, KEK
1-1 Oho, Tsukuba-shi, Ibaraki, 305, Japan

April 24, 1995

Abstract

We describe a new method to measure a nanometer beam size during collisions at future e^+e^- linear colliders by using e^+e^- pairs. A huge number of pairs are deflected in a strong Coulomb potential made by an oncoming beam. Since the potential is a function of the beam size(σ_x,σ_y), the pairs are expected to carry this information, especially in their angular distributions. We investigated this process in detail by a simulation use of ABEL under realistic experimental conditions as well as by analytic studies. Besides the beam size, a vertical displacement between two beams and rotations in the transverse beam profile can be precisely measured. Because of the high statistics of pairs, the results from these measurements can be used for feedback during real-time operation of linear colliders.

1 Introduction

In future e^+e^- linear colliders it is essential to have very flat beams at the interaction point (IP) in order to obtain high luminosity. The typical beam size is 3nm(σ_y) x 260nm(σ_x) at IP for the Japan Linear Collider (JLC-I)[1]. A measurement of the beam size is extremely important from the view point of beam diagnostics, especially to maintain the stable operation of linear colliders[2]. Although several ideas have been presented for this purpose, none of them can be used at IP. Recently, T.Shintake has proposed a nanometer beam-size monitor utilizing backward Compton scattering of interfering laser light, which can be used to measure the beam size down to 5nm[3]. We can not measure with certainty 3nm or smaller size, even with this method. So far, there has been no idea of how to clearly measure such a small beam size, much less to measure it during a collision.

*KEK preprint 94-122, revised on 1/26/1995 when this paper was re-submitted to PR-E.

In this paper we describe a completely new idea for measuring the beam size at IP. As is well known, many low-energy e^+e^- pairs are expected to be created during beam crossing due to three incoherent processes: the Breit-Wheeler (BW:$\gamma\gamma \rightarrow e^+e^-$) process, the Bethe-Heitler (BH: $e^{\pm}\gamma \rightarrow e^{\pm}e^+e^-$) process and the Landau-Lifshitz (LL: $e^+e^- \rightarrow e^+e^-e^+e^-$) process, where γ is a beamstrahlung photon. These phenomena have been investigated as troublesome background for experiments at future linear colliders[4]. The particles of our concern have the same charge as that of the oncoming beam, and are hereafter called "same-charge" particles. Most of them are deflected at larger angles than their inherent scattering angles by a strong electromagnetic force due to the oncoming beam, while the "opposite-charge" particles must oscillate inside the oncoming beam because of a focussing force between them; they are deflected with small angles. Figure 1 shows a schematic view of these phenomena. They can be well described by a scattering

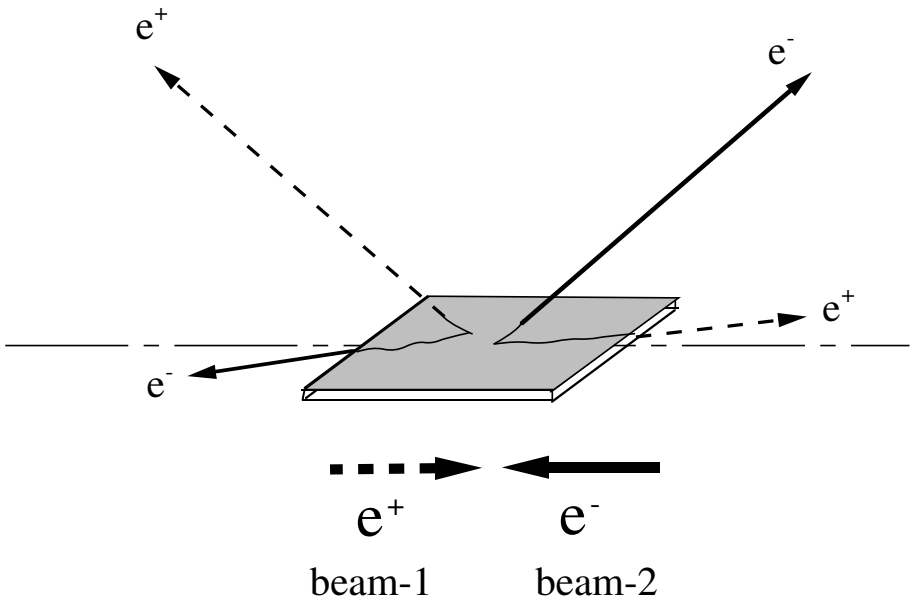

Figure 1: Schematic view of e^+e^- pair creations and deflections during a collision, where two flat beams are depicted as overlapping sheets at IP and two $e^{\pm}$ pairs are created in forward and backward angles, only as an example.

process of $e^-(e^+)$ in a two-dimensional Coulomb potential which is Lorentz-boosted to the rest frame of the oncoming beam[5]. Since this potential is produced by the intense electric charge of the oncoming beam, it is a function of the transverse size (σ_x,σ_y) and intensity of the beam. Therefore, the deflected particles should carry this information, especially in their angular distribution, which we intend to measure. It should be noted that we can measure the sizes of the two beams independently, since the particles must be deflected asymmetrically in the forward and backward angular regions if the two beams have different beam parameters, *i.e.* there are two independent Coulomb potentials of the two beams separated by a large Lorentz-boost along the beam axis. Moreover, we can measure the relative

displacement and transverse rotation of two beams. In addition, this measurement will provide a real-time, fast feedback to collider-machine operation at the same time that experiments are being conducted.

In subsequent sections we describe an analytic expression for the angular distribution of elliptic beams, where the charge density is uniform inside an elliptic cylinder, since only this case can be calculated analytically, and, further, it explains most of the features for Gaussian beams under the beam-beam effects at IP. We then present the results of a simulation using the ABEL program[6, 4], which takes account of all known beam-beam effects, for the case of JLC-I as an example of future linear colliders.

2 Analytic Calculation for Elliptic Beams

The equation of motion of a same-charge particle during a beam-beam collision is expressed by[5]

$$\frac{d^2x}{dt^2} = \frac{4Nr_e}{\gamma\epsilon}\frac{1}{2L}\frac{\partial\Phi}{\partial x} \tag{1}$$

(similarly for y), where N is the beam intensity, $2L$ the bunch length, r_e the classical electron radius, γ the Lorentz factor of the beam energy and ϵ the energy fraction of the particle. For a uniform charge distribution inside an elliptic cylinder of $2L$ long with radii a and b in the horizontal(x) and vertical(y) directions, respectively, the Coulomb potential is exactly given by

$$\Phi = \begin{cases} \frac{1}{a+b}\left(\frac{x^2}{a}+\frac{y^2}{b}\right) & \left(\frac{x^2}{a^2}+\frac{y^2}{b^2}\le 1\right) \\ \log\frac{\sqrt{a^2+q}+\sqrt{b^2+q}}{a+b} + \frac{x^2/\sqrt{a^2+q}+y^2/\sqrt{b^2+q}}{\sqrt{a^2+q}+\sqrt{b^2+q}} & \left(\frac{x^2}{a^2}+\frac{y^2}{b^2}>1\right), \end{cases} \tag{2}$$

where $q(x,y)$ is the positive solution to the equation $x^2/(a^2+q)+y^2/(b^2+q)=1$. Assuming that a particle is created uniformly at a position $(x_\circ, y_\circ)$ with zero scattering angle ($\dot{x}_\circ = \dot{y}_\circ = 0$), its trajectory inside the ellipsoid is

$$x = x_\circ \cosh\omega_x t, \qquad \omega_x^2 = \frac{4Nr_e}{\gamma\epsilon L}\frac{1}{a(a+b)} \tag{3}$$

$$y = y_\circ \cosh\omega_y t, \qquad \omega_y^2 = R\,\omega_x^2, \tag{4}$$

where $R \equiv a/b$ is the aspect ratio of the transverse beam profile, which is equivalent to σ_x/σ_y for a Gaussian beam.

We first consider the azimuthal angular distribution of same-charge particles while ignoring the Coulomb field outside of the cylinder. The azimuthal angle (ϕ) is defined by

$$\phi = \tan^{-1}\frac{\dot{y}}{\dot{x}} = \tan^{-1}\frac{1}{\sqrt{R}}\frac{\eta_\circ}{\xi_\circ}\frac{\sinh\tau}{\sinh\frac{\tau}{\sqrt{R}}}, \tag{5}$$

where

$$\tau = \omega_y t, \quad \xi_\circ = \frac{x_\circ}{a} = \frac{\cos\phi \sinh\tau}{\sqrt{A}}, \quad \eta_\circ = \frac{y_\circ}{b} = \frac{\sqrt{R}\sin\phi\sinh\frac{\tau}{\sqrt{R}}}{\sqrt{A}}, \text{ and}$$
$$A = (\cos\phi\sinh\tau)^2 + R(\sin\phi\sinh\frac{\tau}{\sqrt{R}})^2 \tag{6}$$

under the condition

$$\xi_\circ^2\cosh^2\frac{\tau}{\sqrt{R}} + \eta_\circ^2\cosh^2\tau = 1 \qquad (i.e.\ \ \frac{x^2}{a^2} + \frac{y^2}{b^2} = 1). \tag{7}$$

The distribution function ($F(\phi)$), which is normalized to unity, is expressed by

$$F(\phi) = \int_0^{+\infty} d\tau \frac{\Theta(1-\xi_\circ^2-\eta_\circ^2)}{\pi}\frac{\partial(\xi_\circ,\eta_\circ)}{\partial(\phi,\tau)}$$
$$= \frac{1}{\pi}\int_0^{+\infty}\frac{d\tau}{\sinh\tau cosh\frac{\tau}{\sqrt{R}}} R\tanh^2\frac{\tau}{\sqrt{R}}\frac{\frac{1}{R}\cos^2\phi + \sin^2\phi(\sqrt{R}\tanh\frac{\tau}{\sqrt{R}}\coth\tau)}{\left[\cos^2\phi + \sin^2\phi(\sqrt{R}\tanh\frac{\tau}{\sqrt{R}}\coth\tau)^2\right]^2}, \tag{8}$$

where Θ is a step function. For $R(\gg 1)$ and $\phi \sim 0$ (or π), where we are interested in measuring the aspect ratio for future linear colliders, $F(\phi)$ can be well approximated as

$$F(\phi) \sim \frac{1}{\pi}\int_0^{+\infty} d\tau \frac{\tau^2}{\sinh\tau}(\frac{1}{R} + \phi^2\tau\coth\tau). \tag{9}$$

As can be clearly seen in the above equations(8,9), the distribution in the angular region near to the horizontal plane is depleted for a large aspect ratio as $1/R$. On the contrary, the distribution in the vertical direction ($\phi \sim \pi/2$) has apparently no dependence on R. Therefore, we hereafter concentrate on calculations near to the horizontal plane in this section. We then estimate the effect of the Coulomb force outside of the elliptic cylinder, where the equation of motion is approximated for $y \sim 0$ and $b \ll a$, as follows:

$$\frac{d^2x}{dt^2} \simeq \ \omega_x^2(x - \sqrt{x^2-a^2}) \tag{10}$$

and

$$\frac{d^2y}{dt^2} \simeq \ \omega_y^2 y^2 \frac{b}{\sqrt{x^2-a^2+b^2}}\frac{a}{x+\sqrt{x^2-a^2}}. \tag{11}$$

Since the vertical force in Eq.(11) is very small in this region, except for $x \sim a$, we neglect it for the moment. Integrating the x component of Eq.(10) once, for large $x \equiv X \gg a$ we obtain

$$\dot{x}^2 \simeq \omega_x^2 a^2 C + \dot{x}_1^2, \tag{12}$$

where $C = \ln\frac{2X}{a} - \frac{1}{2}$ and $\dot{x}_1 \equiv \omega_x a\sqrt{1-\xi_\circ^2}$, which is the x-velocity at the position $(x,y) = (a,0)$. The resultant distribution function at $\phi = 0$ is give for large $R \gg 1$ by

$$F(0) = \frac{1}{\pi}\int_0^{+\infty} \frac{1}{\sqrt{R}}\frac{\tau d\tau}{\sinh\tau}\sqrt{C} = \frac{\pi\sqrt{C}}{4}\frac{1}{\sqrt{R}}. \tag{13}$$

We further estimated the effect of the vertical force neglected in the above calculation by numerically integrating Eqs.(10) and (11). The major effect was found to be an overall change in the magnitude by a constant factor of $\sim 1/4.5$. Therefore, the R dependence of $F(0)$ becomes $1/\sqrt{R}$ instead of $1/R$ (Eq.(9)) mainly due to a horizontal force outside of the elliptic cylinder. Thus, for the case of a flat beam ($\sigma_x/\sigma_y \gg 1$), the same-charge particles are strongly deflected in the vertical direction; their azimuthal angular distribution gives us direct information about R. It should also be noticed that the particles tend to be deflected more in a direction where their creation points are displaced by Δ_x and Δ_y, since the forces are proportional to $(x+\Delta_x)/\sigma_x$ and $(y+\Delta_y)/\sigma_y$, respectively, provided by differentiating Eq.(2). This gives us the sensitivity to measure the alignment between two beams, which is discussed in the next section.

The maximum deflection angle for low-energy particles can be expressed by[5]

$$\theta_x^{max} \sim \theta_y^{max} \sim \left[\frac{\ln(\frac{4\sqrt{3}D_x}{\epsilon})}{\sqrt{3}\epsilon D_x}\right]^{1/2}\theta_\circ \propto \frac{1}{\ln\sigma_x}\ (R\to\infty), \tag{14}$$

where $\sigma_x = a/2$, $\sigma_y = b/2$, $\sigma_z = 2L/\sqrt{3}$ and $\theta_\circ \equiv 2Nr_e/(\gamma(\sigma_x+\sigma_y)) = D_x\sigma_x/\sigma_z$. Using these relations, Gaussian beams $(\sigma_x,\sigma_y,\sigma_z)$ can be well described in terms of variables (a,b,L) of an elliptic cylinder. Assuming that the beam intensity and the bunch length are known, the horizontal beam size can be obtained from a measurement of the maximum deflection angle, especially for a large aspect ratio, as can be clearly seen in Eq.(14).

3 Simulation by ABEL

3.1 Beam-beam effect

In order to investigate our method quantitatively by taking into account all beam-beam effects, which include beam disruption, the horizontal crossing angle, the vertical displacement between two beams, transverse rotations for flat beams and the energy and angular distributions of created pairs *etc.*, we must rely on Monte-Carlo simulations by using ABEL, although the principal dynamics can be well described analytically by an approximation of the elliptic cylinder, as demonstrated in the previous section. A detailed explanation of ABEL can be found in [6, 4]. As an example of a future linear collider we consider JLC-I[1], whose parameters relevant to the simulation are given as follows: the beam energy (E_b) is 250GeV and the intensity (N) is 10^{10}/bunch; Gaussian beams with $\sigma_x^\circ/\sigma_y^\circ = 260./3.04$ nm, $\sigma_z^\circ = 80\mu$m, the

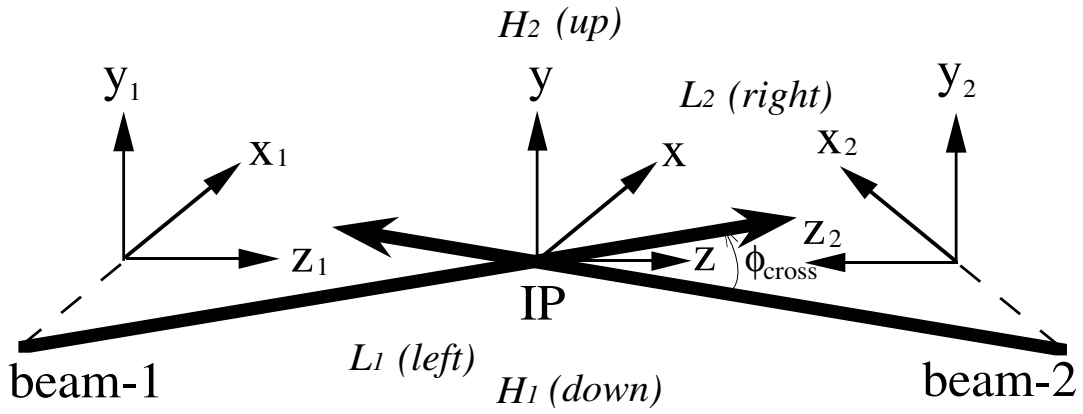

Figure 2: Coordinate system used in ABEL, where z_1, z_2 and z are collinear. The trajectories of the beam-centers are indicated by the long/thick arrows.

horizontal crossing angle ϕ_{cross} = 8mrad and the luminosity $L = 9.7 \times 10^{33}$ cm^{-2} sec^{-1} with 72 bunches/pulse at the frequency of 150 Hz.

We first define the coordinate system used in ABEL. There are three kinds of coordinate systems shown in Fig.2. Two of them, (x_1, y_1, z_1) and (x_2, y_2, z_2), move together with beam-1 (positrons) and beam-2 (electrons), respectively. The former is a left-handed system, while the latter is a right-handed system. The third one, (x, y, z), is the rest frame at IP. All three coordinates are collinear in the z-direction. In the presence of crossing, the origins of the moving systems are shifted from the centers of the beams, except in the z_1- and z_2- directions, as shown in Fig.2. The crossing angles of two beams are +4mrad, each in the directions of x_1 and x_2, that is 8mrad (ϕ_{cross}) between them. Since we expect a large asymmetry in the azimuthal angular distribution of the deflected particles, especially in the vertical-horizontal asymmetry for flat beams, as explained in the previous section, we define 4 azimuthal angular regions in Fig.2 (L_1, L_2, H_1 and H_2) corresponding to left, right, down and up, respectively, as seen from the upstream of beam-2.

The e^+e^- pairs are generated from three processes (BH, BW and LL), where the energies of the particles are more than 5 MeV; they are tracked with all of the effects during a beam-beam crossing by ABEL[4]. After the crossing, the azimuthal angular distribution is plotted for particles whose energies (E_e) and deflection angles (θ_e) are more than 100 MeV and 20 mrad, respectively, in Fig.3 (a), which is compared to the case of a head-on collision, *i.e.* the zero horizontal crossing angles shown in Fig.3 (b). Hereafter, we always show the azimuthal angles measured downstream from beam-1, that is, those of the particles deflected by beam-2, since the distributions are symmetrical at both sides of IP for the same parameters of the two beams. As can be clearly seen in Fig.3, electrons of the pairs, which have the same charge as those of beam-2, are strongly deflected in the vertical direction, while the positrons show only a moderate suppression in the horizontal plane, as indicated by the shaded area in this figure. We can also see the effect of the 8mrad crossing with a tendency of deflecting more to the right. This shows a general feature, that is, when particles have a finite initial angle they are deflected more in this direction. The crossing

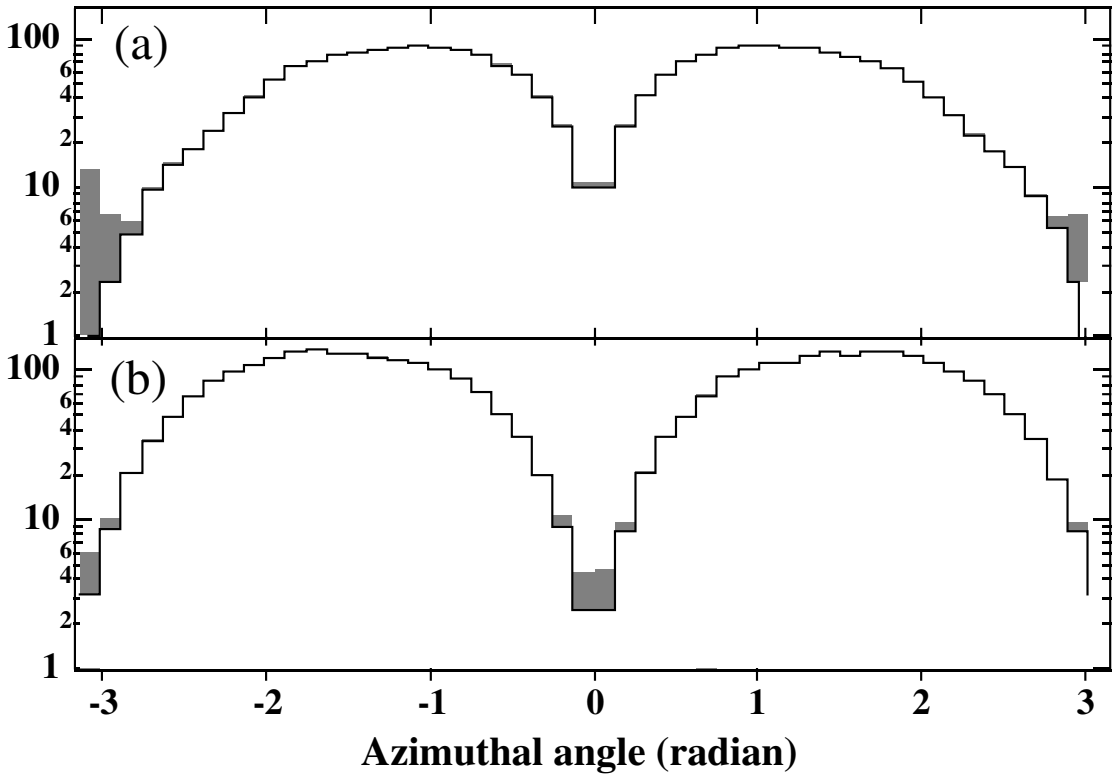

Figure 3: (a) Azimuthal angular distribution of deflected electrons and positrons($E_{e\pm} > 100$MeV, $\theta_{e\pm} > 0.02$) for JLC-I. The shaded area corresponds to that of those positrons which are oppositely charged particles as that of the oncoming beam. (b) The same as (a) except for a zero horizontal crossing angle, *i.e.* for a head-on collision. The vertical scale is the number of particles per single-bunch crossing.

angle generates a horizontal displacement (Δ_x) uniformly over the particles at a very early stage of their deflections. The certain displacement of Δ_x is the origin of this feature, as mentioned in the previous section.

Since the created particles have inherent scattering angles (θ_e°) of typically m_e/E_e, where m_e is the electron mass, an effect due to these angles is also expected. It has been found to produce a deeper depletion in the horizontal direction than speculated in the previous section, where the inherent angle was neglected. $F(0)$ (also $F(\pm\pi)$) is now nearly proportional to $1/R$ rather than to $1/\sqrt{R}$ in Eq.(13), as can be seen in Fig.4. In this figure the azimuthal angular distribution for the nominal

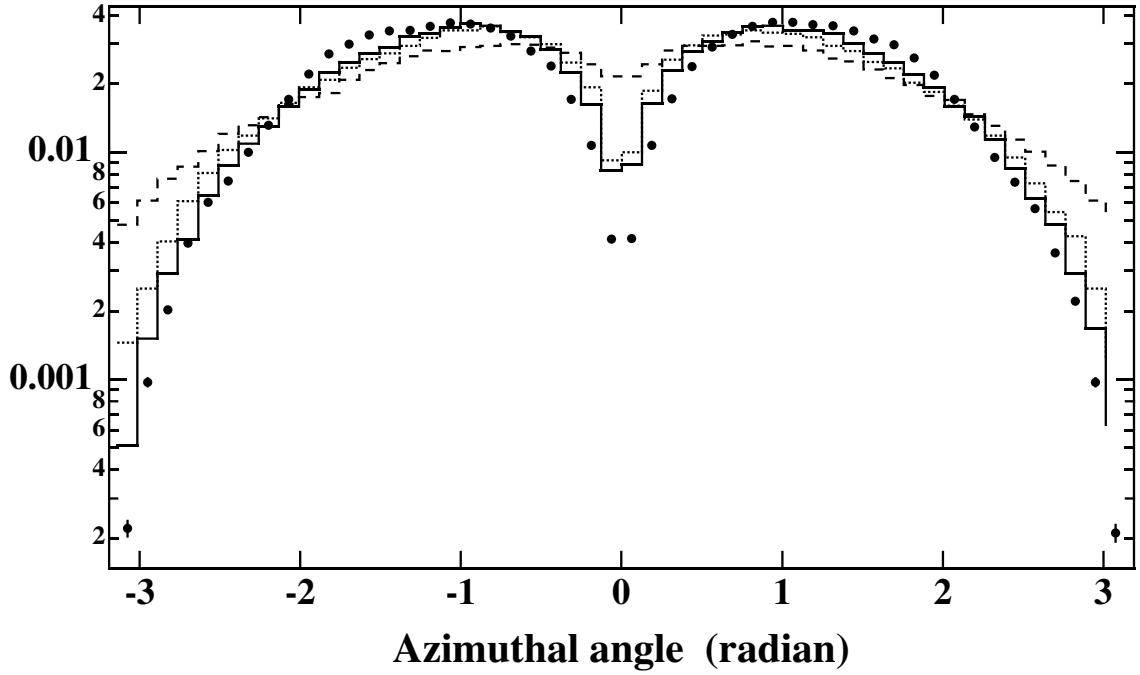

Figure 4: Azimuthal angular distributions of deflected electrons ($E_e > 100$MeV, $\theta_e > 0.02$), whose charges are the same as that of beam-2 for JLC-I with nominal parameters (solid circles) together with three cases ($\sigma_y = 2\sigma_y^\circ$(solid line), $3\sigma_y^\circ$(dotted one) and $10\sigma_y^\circ$(dashed one)) in which the other beam parameters are the same as those of the nominal beam. The distributions were normalized by the total number of electrons in them.

JLC-I parameters is compared with three cases ($\sigma_y = 2\sigma_y^\circ, 3\sigma_y^\circ$ and $10\sigma_y^\circ$), where the other parameters are the same as the nominal ones and only those electrons of $E_e > 100$MeV and $\theta_e > 0.02$ are plotted in order to see the depletion more clearly as a function of σ_y.

3.2 Tracking in a solenoidal magnetic field

In order to estimate the actual sensitivity, we must take into account the helical trajectory in the solenoidal magnet of the detector. We assume a uniform field of 2 Tesla parallel to the z-axis. We detect the particle positions 1m downstream from

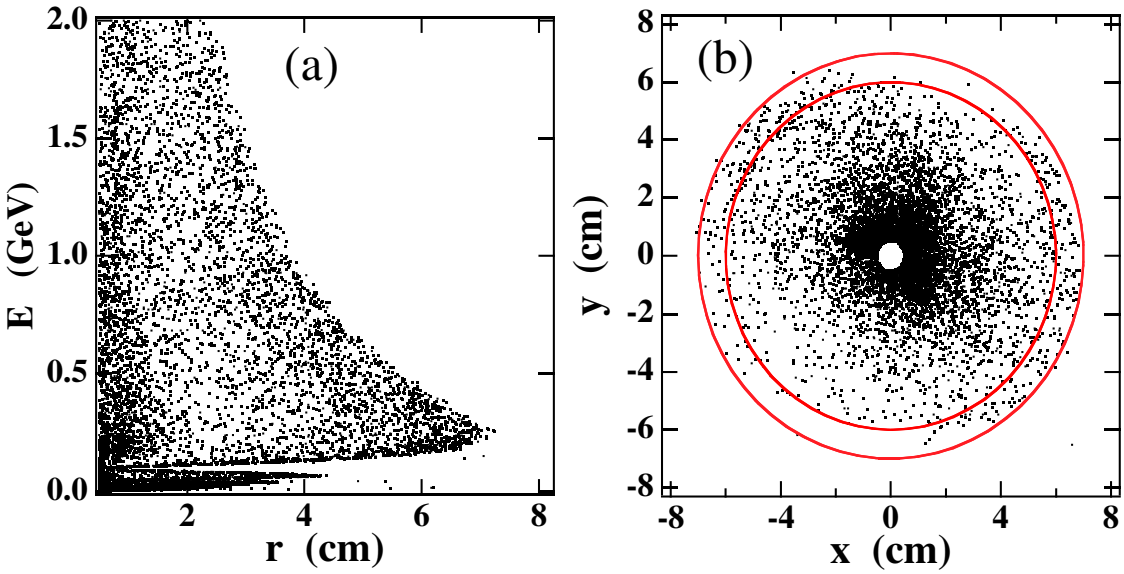

Figure 5: Distributions of scattered particles at $z = +1$m, where particles with $r > 0.5$cm are plotted. The particles are tracked in helical trajectories in a magnetic field of B_z=2 tesla. (a) is for a scatter plot on the plane of the energy(E) and the radial distance(r), and (b) is for a plot on the plane of x and y, where two concentric circles of 6 and 7cm radii are also shown just for an eye guide.

the IP,*i.e.* $z = +1$m. Figures 5(a) and (b) show the radial and azimuthal angular distributions of the particles, respectively. There is a clear maximum radial boundary as a function of the energy in Fig.5(a), as expected from the Eq.14. Outside of the boundary only a relatively small number of the particles can be seen, which have inherent angles larger than the beam-beam deflection angle. We can also see another dense region at r <1 cm corresponding to the opposite-charge particles(e^+), as described in the previous section. The most interesting particles are distributed at the maximum radial distance of around r=7cm. Since they have almost the same magnitude as the energy, as clearly shown in Fig.5(a), their original azimuthal distribution should be preserved even after they flowed in the magnetic field. Actually, this expectation is realized as in Fig.5(b), where we can clearly see two sides of the depleted region, especially for 6< r <7cm. The two sides are sitting on a line rotated counter-clockwise by ∼70°, which corresponds to the horizontal direction.

3.3 Results

3.3.1 Measurement of σ_x

The maximum radius (r_{max}) seen in Fig.5(a) corresponds to the maximum deflection angle, since most of the particles obtain transverse momenta mainly due to deflection. Therefore, from a measurement of r_{max} we can obtain information concerning σ_x (see Eq.14). A simulation has confirmed that r_{max} depends mainly on σ_x, at least for σ_y <10 σ_y°, as shown in Fig.6, where r_{max} can be defined as the shoulder;

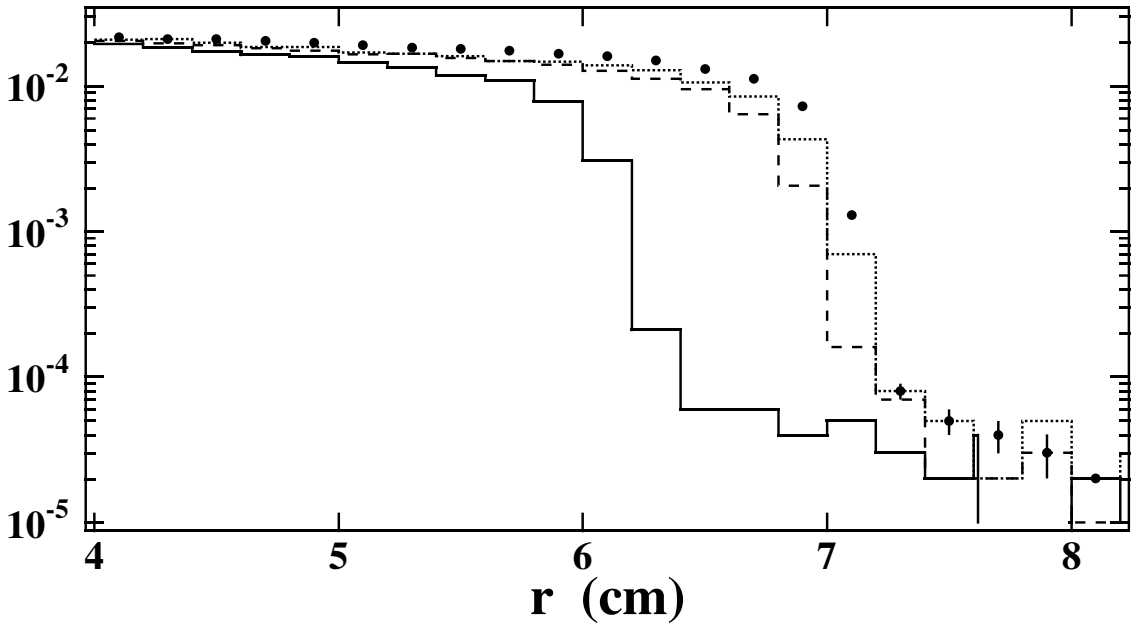

Figure 6: Radial distribution of scattered particles at $z = +1$m. The solid circles are those of the nominal beam condition; the dotted, dashed and solid lines are those of σ_y=$2\sigma_y^\circ$, σ_y=$10\sigma_y^\circ$ and σ_x=$2\sigma_x^\circ$, respectively, where the other beam parameters are the same as those of the nominal beam. The distributions are normalized by the total number of particles of E >100MeV.

r_{max}=7.1 and 6.1cm for the nominal and the case of twice wider σ_x, respectively. Small tails due to scattering with large inherent angles are also observed beyond the shoulders. The ratio $r_{max}(2\sigma_x^\circ)/r_{max}(\sigma_x^\circ)$ is found to be 0.86, which should be compared with 0.88 estimated by Eq.14. In order to estimate σ_x from the observed r_{max} we have to know the beam intensity (N); it can be accurately measured by using monitors in the accelerators. We therefore expect a very good on-line measurement of σ_x.

3.3.2 Measurement of σ_y

Figure 7 shows the azimuthal angular distributions measured for $6< r < 7$cm at $z = +1$m for various values of σ_y's, where 4 angular regions are defined for further numerical studies, *i.e.* L_1(left)$\equiv -2.135 \sim -1.633$, L_2(right)$\equiv$ $1.005 \sim 1.507$, H_1(down)$\equiv -0.502 \sim 0.126$ and H_2(up)$\equiv$ $2.261 \sim 2.889$. By comparing this figure with Fig.4 we can clearly see that the linear dependence on R of the yields in the depletion region is preserved through the motion in the solenoid. The effect of the horizontal crossing can still be seen in Fig.7; that is, there is more depletion on the left side(L_1) than on the right (L_2). The numbers of particles are expected to be 2.4, 3.5, 120, and 120 per single-bunch crossing in L_1, L_2, H_1 and H_2, respectively, under the nominal beam condition. The statistics will actually be much better because the beam pulse contains 72 bunches. Thus, there will be no problem in the statistical sensitivity for this measurement, although the yields decrease inversely proportional

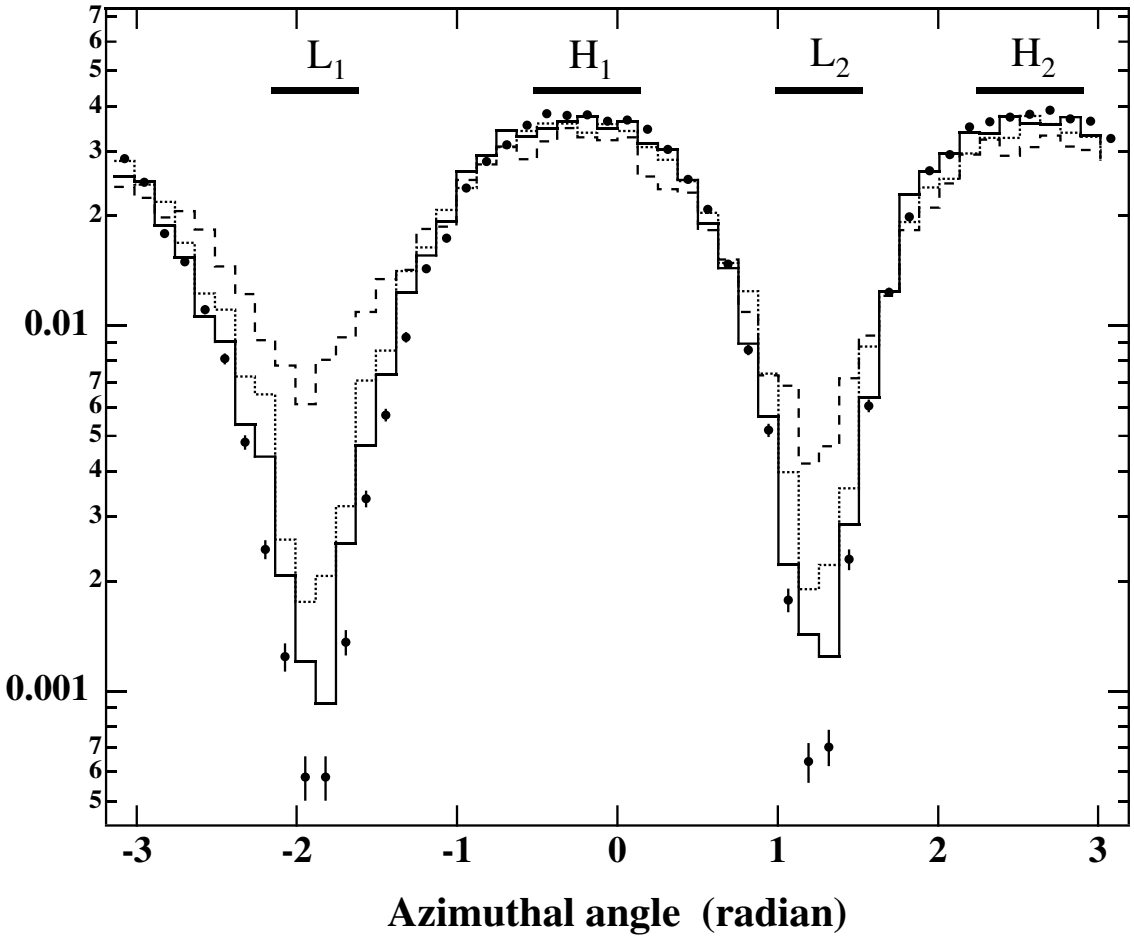

Figure 7: Azimuthal angular distributions measured for $6< r < 7$cm at $z = +1$m for R =85.5(solid circles), 42.8(solid line), 28.5(dotted one) and 8.55(dashed one) corresponding to $\sigma_y = \sigma_y^\circ$, $2\sigma_y^\circ$, $3\sigma_y^\circ$ and $10\sigma_y^\circ$, respectively. The distributions are normalized by the total number of particles. The angular regions of L_1(left), L_2(right), H_1(down) and H_2(up) are also shown.

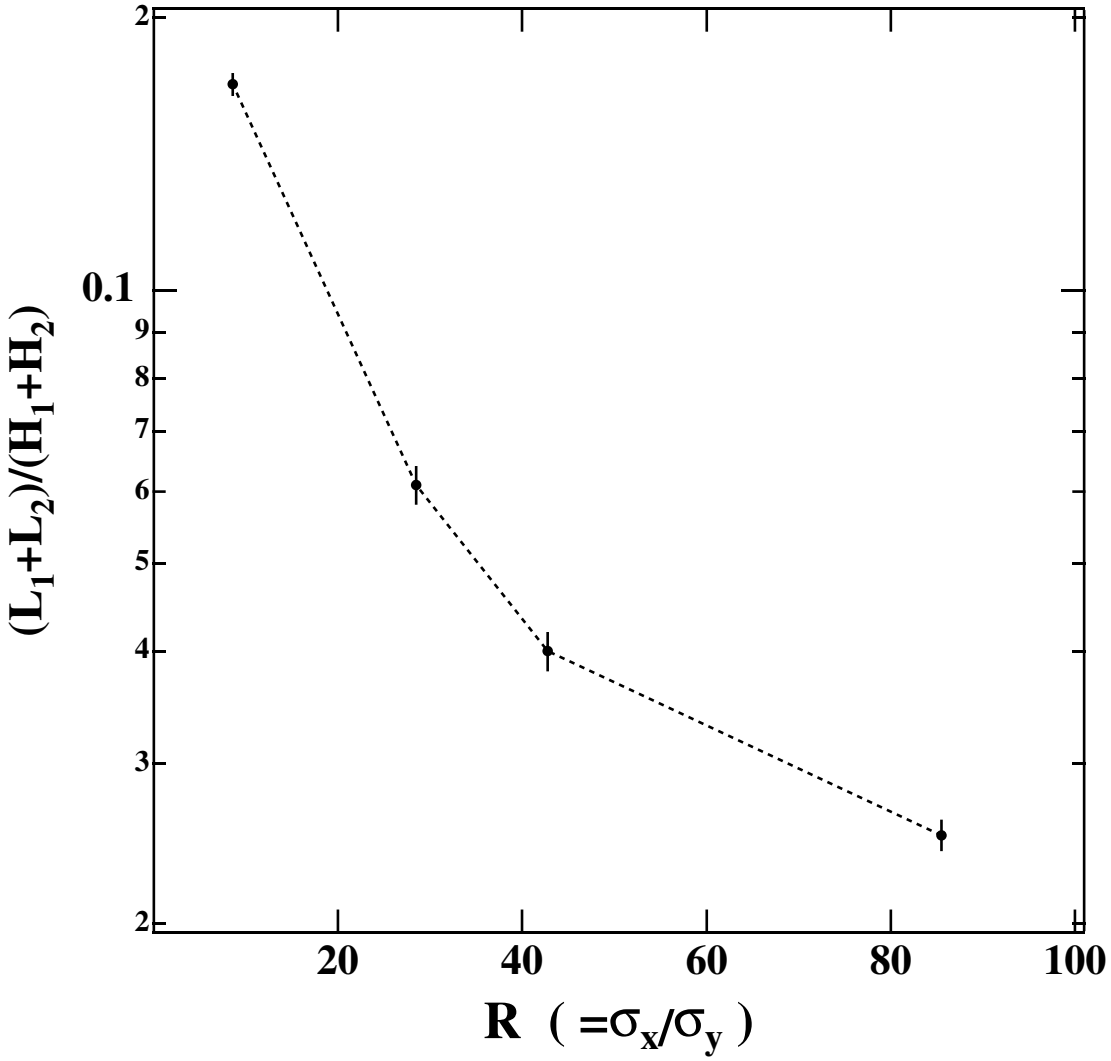

Figure 8: Number of particles in L_1 and L_2 normalized by that in H_1 and H_2 as a function of R. The same data are used as in the previous figure. The errors are statistical, corresponding to 160 bunch crossings, except for the lowest R, which corresponds to 800 bunch crossings.

to σ_y. The ratio of $(L_1 + L_2)/(H_1 + H_2)$ is plotted as a function of R in Fig.8. Actually, this ratio depends only on R, as expected by Eq.13. Since σ_x is measured from r_{max}, we can obtain $\sigma_y (= \sigma_x/R)$ by this azimuthal angular distribution. The statistical accuracy will be less than $0.1\sigma_y^\circ$ with a few pulse-train crossings if no significant background exists.

3.3.3 Measurement of vertical displacements (Δ_y)

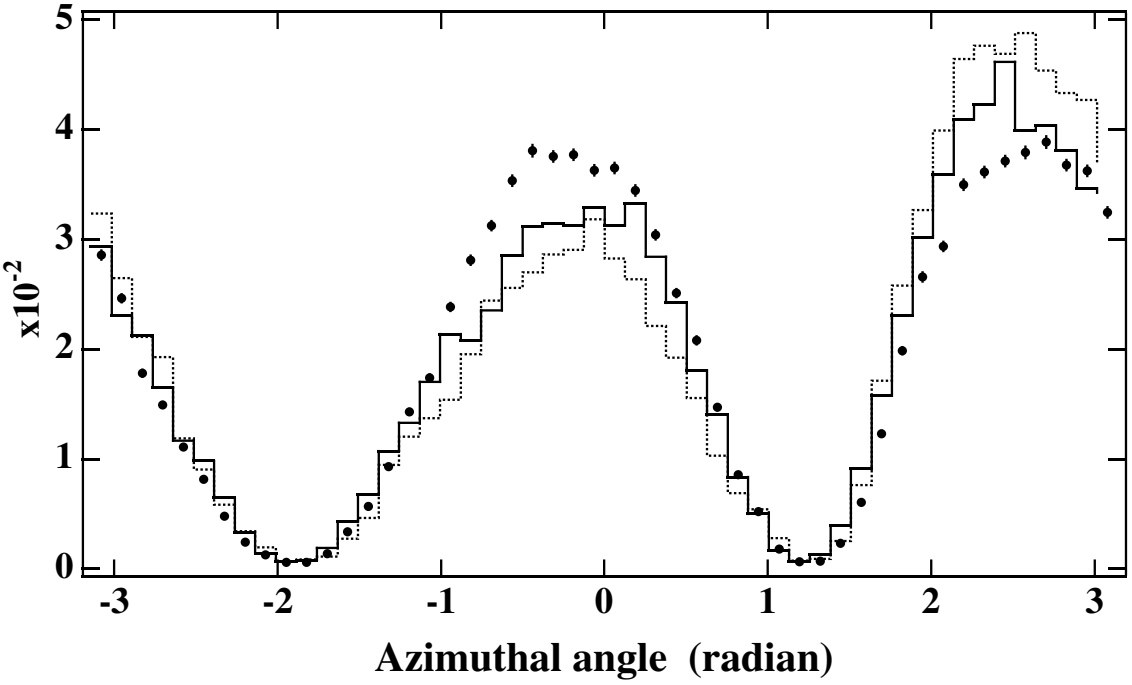

Figure 9: Azimuthal angular distributions measured for $6 < r < 7$cm at $z = +1$m for vertical displacements of $\Delta_y = \pm 0.5\sigma_y^\circ$(solid line), $\pm 1.0\sigma_y^\circ$(dotted line) compared with the nominal one (solid circles). The distributions are normalized by the total number of particles.

When two beams collide with a finite vertical displacement(Δ_y) comparable to σ_y°, we expect a vertical, *i.e.* up-down, asymmetry in the azimuthal angular distribution. In the simulation beam-1 and beam-2 are initially shifted by $+|\Delta_y|$ and $-|\Delta_y|$, respectively. We examined the two cases of $\Delta_y = \pm 0.5\sigma_y^\circ$ and $\pm 1.0\sigma_y^\circ$, and plotted the angular distribution in Fig.9. (The luminosity losses are 6 and 30% for $\Delta_y = \pm 0.5\sigma_y^\circ$ and $\pm 1.0\sigma_y^\circ$, respectively.) Apparently, during a collision the particles are deflected more in the upper side of the electromagnetic field of beam-2, since they are created in the overlapping region between two beams. Therefore, they are deflected more in $+y$ and less in $-y$ than in the nominal case, as can be clearly seen in Fig.9. The ratios H_1/H_2 are found to be 0.76 and 0.62 for $\Delta_y = \pm 0.5\ \sigma_y^\circ$ and $\pm 1\sigma_y^\circ$, respectively.

3.3.4 Measurement of transverse rotation (ϕ_{xy})

Since the beams are very flat because R=85.5 for JLC-1, a small transverse rotation (ϕ_{xy}) of the beam causes a significant loss of luminosity. This effect is enhanced by the presence of the crossing angle. Actually, the luminosities were estimated using ABEL to be 0.93-, 0.80- and 0.55-times the nominal one for ϕ_{xy}=$\pm$0.005, 0.01 and 0.02 radian, respectively, where + and $-$ are for beam-1 and beam-2, respectively. Even for rotation in the same direction, *i.e.* no relative rotation between two beams, similar luminosity losses were obtained. On the other hand, in a head-on collision the luminosity loss is only 20% at most, even for ϕ_{xy}=$\pm$0.02.

First for the opposite rotation the right half of beam-1 with $+|\phi_{xy}|$ traverses above beam-2 with $-|\phi_{xy}|$ during a collision, while the left half traverses below beam-2. Therefore, the azimuthal distribution from the right (left) half of beam-1 has more (less) particles at H_2 than at H_1. If two beams collide head-on, no such up-down asymmetry is expected in the total distribution, since the right- and left-hand sides cancel each other. However, under the presence of a horizontal crossing angle (see Fig. 2), particles on the right-hand side are deflected more than those on the left. We therefore expect an up-down asymmetry of H_1/H_2 <1. The results of the simulation agree with our expectation, as shown in Fig.10. The ratios of H_1/H_2 were obtained to be 0.99, 0.92 and 0.78 for ϕ_{xy}= $\pm$0.005, $\pm$0.01 and $\pm$0.02, respectively.

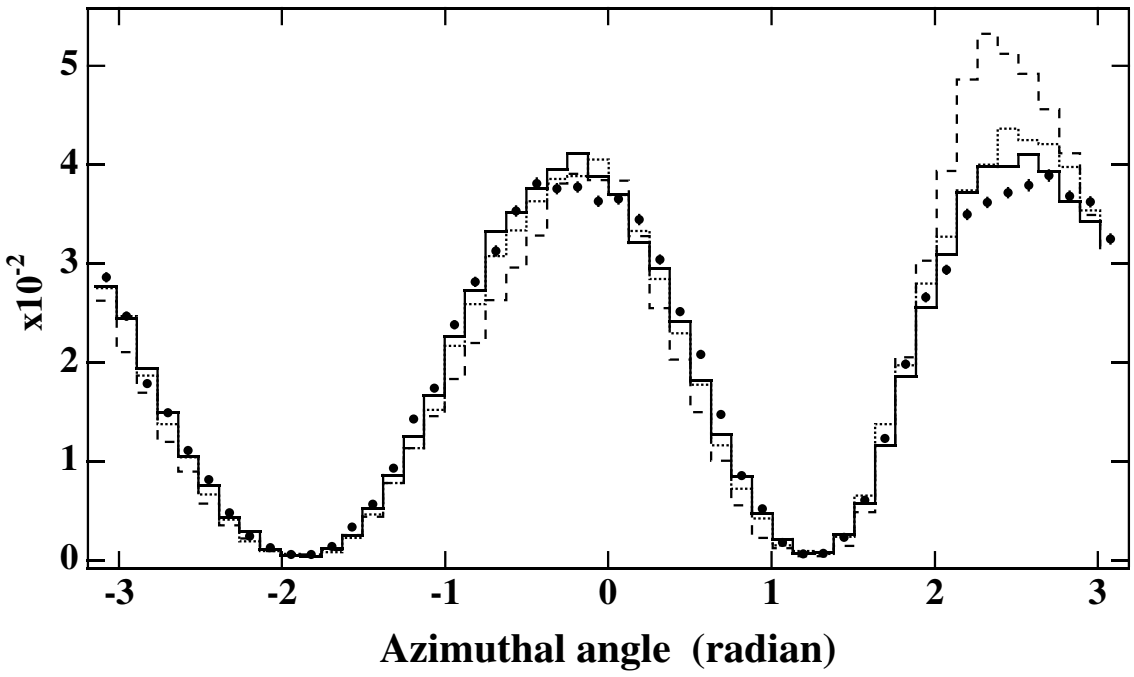

Figure 10: Azimuthal angular distributions measured for 6< r < 7cm at z = +1m for various transverse rotations compared with the nominal one(solid circles). The signs of the rotations in xy plane are opposite for two beams, *i.e.* ϕ_{xy}= $\pm$0.005(solid line), $\pm$0.01(dotted one), $\pm$0.02(dashed one) radian. The distributions are normalized by the total number of particles.

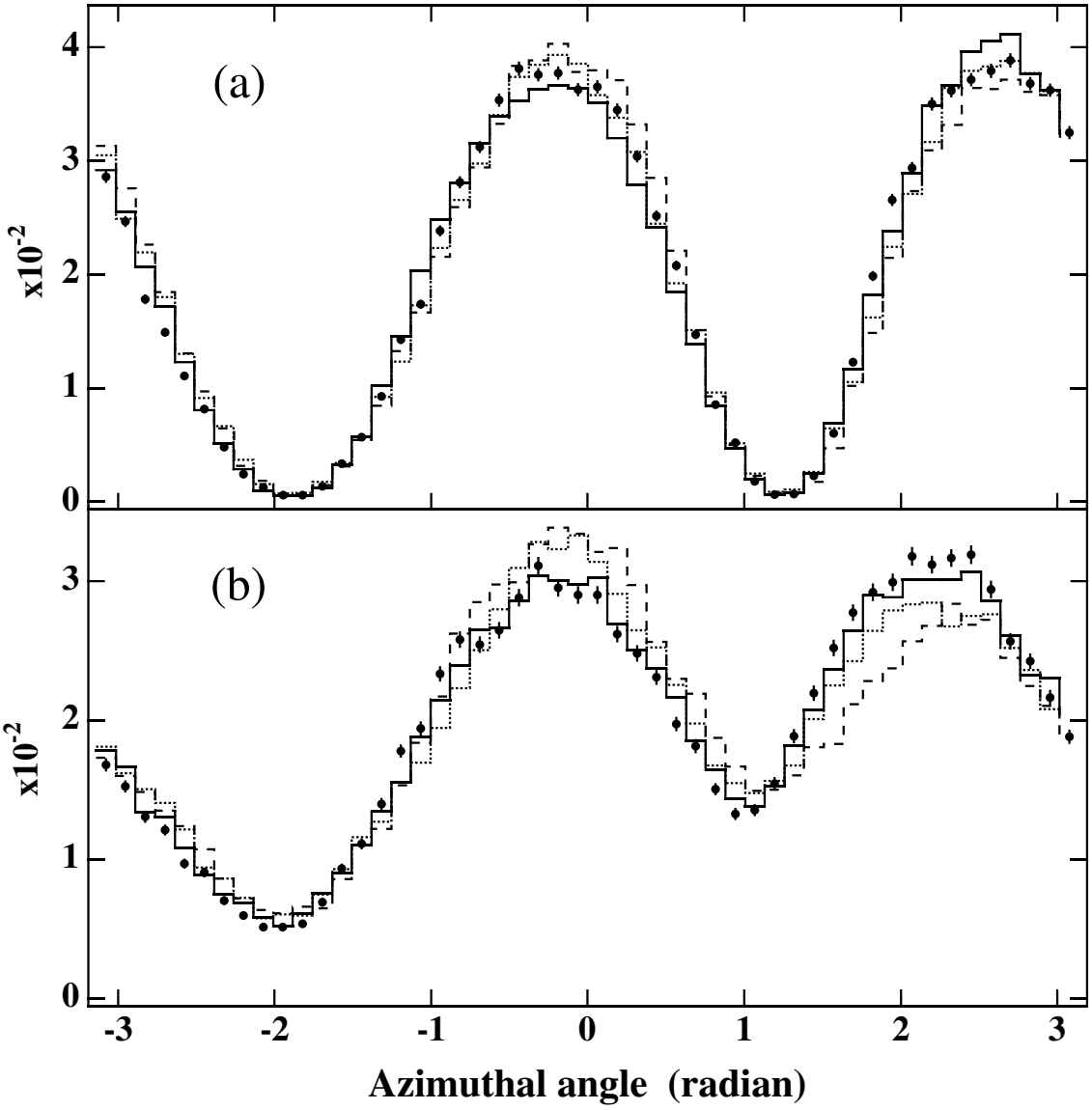

Figure 11: Azimuthal angular distributions measured for (a) 6< r < 7cm and (b) 5< r < 6cm at z = +1m for various rotations compared with the nominal one(solid circles). The magnitudes of the rotations are ϕ_{xy}=+ 0.005(solid line), +0.01(dotted one), +0.02(dashed one) for both beams. The distributions are normalized by the total number of particles.

Table 1: Summary of the results obtained by ABEL for JLC-I at E_{beam}=250GeV. The errors are only statistical, corresponding to the number of bunch crossings listed in the second column. The conditions in the first column show only changed beam parameters, assuming that the others are the same as the nominal one. These conditions are for both beams, unless specified. The upper and lower signs in the first column correspond to beam-1 and beam-2, respectively. In the last column, $H_1' = -0.377 \sim 0.251$ and $H_2' = 2.010 \sim 2.638$ according to a movement of the second peak in the azimuthal angular distributions for $5< r <6$cm.

condition	statistics # bunches	$(L_1+L_2)/(H_1+H_2)$	H_1/H_2 $6< r <7$cm	H_1'/H_2' $5< r <6$cm
nominal (R =85.5)	160.	0.025±0.001	1.00±0.01	0.97±0.01
σ_y=2σ_y° (R =42.8)	160.	0.040±0.002	1.00±0.02	1.01±0.02
σ_y=3σ_y° (R =28.5)	160.	0.061±0.003	1.02±0.02	0.96±0.03
σ_y=10σ_y° (R =8.55)	800.	0.17±0.01	1.05±0.02	0.93±0.02
Δ_y=±0.5σ_y°	80.	0.034±0.001	0.76±0.01	0.69±0.02
Δ_y=±1.0σ_y°	80.	0.031±0.002	0.62±0.01	0.56±0.02
ϕ_{xy}=±0.005	240.	0.024±0.001	0.99±0.01	0.93±0.01
ϕ_{xy}=±0.01	240.	0.020±0.001	0.92±0.01	0.85±0.01
ϕ_{xy}=±0.02	320.	0.015±0.001	0.78±0.01	0.71±0.01
ϕ_{xy}=+0.005	240.	0.024±0.001	0.92±0.01	1.02±0.01
ϕ_{xy}=+0.01	240.	0.031±0.001	1.00±0.01	1.17±0.02
ϕ_{xy}=+0.02	320.	0.027±0.001	1.08±0.01	1.37±0.02

Secondly, for the same rotation case, beam-1 traverses beam-2 from its top(bottom) surface to its bottom(top) surface if the sign of the rotation is positive(negative). We may expect an enhancement at the down(up) side due to the crossing angle from the same arguments as in the case of the opposite rotation. The simulation shows slight enhancements in the distribution for $6< r < 7$cm, as can be seen in Fig.11(a), while the distribution for smaller radii, $5< r < 6$cm, has clear up-down asymmetries for $\phi_{xy} >0.01$, as shown in Fig.11(b). The reason for this radial dependence can be explained based simply upon geometrical considerations as follows. During a collision the vertical displacement between the two beams is approximately a linear function of z_1 and z_2 (Fig.2) as well as ϕ_{xy}. The particles measured for $6< r < 7$cm are really created in the central region of the collision,*i.e.* within about $1/3\sigma_z$ in $z_{1(2)}$, where the vertical distance is very close to zero. The particles measured at smaller radii should be created over a wider region along z_1 with a significant amount of vertical displacement. Thus, the sensitivity against ϕ_{xy} in up-down asymmetries increases as r becomes smaller. However, there is a certain limitation because of the poor monochromaticity of particles energies at smaller r, as can be seen in Fig.5(a).

Finally, we summarize all of the results in Tab.1. Here, although we show the cases of particular signs of displacements and rotations, the results for the opposite

signs are simply obtained by exchanging H_1 and H_2. And although both the vertical displacements and the transverse rotations produce up-down asymmetries in H_1/H_2, the separation between them is evident, as can be seen in Figs.9,10 and 11.

4 Feasibility of measurements

At present the most promising detector is a pixel type such as CCD vertex detectors[7] in order to measure dense positions of particles. We do not need to measure their energies since momenta of our interesting particles are analyzed by the 2 tesla solenoidal magnetic field as described in the previous section. The densest regions are H_1 and H_2, whose density is estimated to be 120(particles) x 72(bunches) /4.1cm^2 (0.32MHz/cm^2) if the detector can be read out only between RF pulses at 150Hz for the JLC-I[9]. The occupancy rate is below 1% in the CCD-detector with 25x25μm^2 pixel size. Assuming that the energy of electrons(positrons) traversing the detector is 200MeV, the total dose is estimated to be 110Krad for a year(100days)'s experiment. This estimated dose is very close to present life time of CCD-detectors. For experiments in several years, we should need more radiation-hard CCD detectors resisting up to 1Mrad. Since there are good prospects, megarad hard CCD detectors are available in the near future[7, 8]. In order to get any useful information inside a bunch-train of 201.6nsec (2.8ns x 72bunches), it is greatly required to have a fast-gating CCD. Since there is few possibilities to realized such a CCD in future, it is very difficult to extract informations for each bunch during collisions. However, there is a solution to get information inside the bunch-train when one of two LINACs can be operated with a single bunch which is called a test beam. This test beam can probe inside the bunch-train in the other LINAC by colliding with the specific bunch in it at IP. We can easily choose any bunch to be probed in the train by adjusting a timing of the test beam. For this test beam operation, any information concerning a bunch property can be obtained.

As clearly seen in Tab.1, where measurement errors are statistical ones corresponding to numbers of bunch collisions listed in the second column, beam sizes (σ_x, σ_y) and vertical displacements can be measured sufficiently even for a single bunch. For the measurements of transverse rotations a few bunch trains must be necessary for the statistical accuracy.

5 Conclusions

We have shown by detailed simulations using ABEL that e^+e^- pairs, especially their azimuthal angular distributions, carry very important information for the measurement of nanometer beam sizes. At first sight, the results are surprising, since it has been expected to be impossible to preserve such information under a large disruption of beams at IP. The reason for the preservation is the large deflection angles of low-energy pairs. Especially the same-charge particles in the pairs are deflected strongly due to the repulsive force of the oncoming beam. Escaping from the beam

immediately after their creation, they continue to feel an electromagnetic field just during a collision where the beam is not disrupted very much.

The simulations have taken place under realistic experimental conditions for the JLC-I(E_{beam}=250GeV), such as a horizontal beam crossing(ϕ_{cross}=8mrad) and a solenoidal magnet of 2 Tesla. Employing particles deflected with maximum angles, we have explicitly demonstrated the possibility of precise measurements of the horizontal beam size(σ_x), the aspect ratio(R), the vertical displacement(Δ_y) and the transverse rotation(ϕ_{xy}). Actually, from measurements of σ_x and R, a vertical beam size of nanometers can be obtained. Since the statistical accuracies of the measurements are sufficient at least with a single pulse-train crossing, *i.e.* at 150Hz, this method will be very useful for a real-time feedback operation to realize stable collisions between nanometer beams at linear colliders. Although the simulations have been executed for the JLC-I as a typical future linear collider, the method can be applied directly for other linear colliders.

5.1 Acknowledgments

The authors are grateful to the Final Focus and Interaction Region sub-group in the JLC working group for very useful discussions. They also thank Professors S.Iwata and K.Takata at KEK for their encouragement to complete this analysis.

References

[1] JLC group, "JLC-I", KEK Report 92-16, December 1992. In this paper we took the parameters of the c-band accelerator for the JLC-I.

[2] R.A. Erickson,"Monitoring in future e^+e^- colliders",SLAC-PUB-4974, May 1989.

[3] T. Shintake, "Proposal of nano-meter beam size monitor for e^+e^- linear colliders", *Nucl. Instr. Meth.* **A311**, 453 (1992). For the other methods, see references therein.

[4] T. Tauchi, K. Yokoya and P. Chen, *Particle Accelerators* **41**, 29 (1993).

[5] K. Yokoya and P. Chen, "Beam-beam phenomena in linear colliders", lecture at 1990 US-CERN School on Particle Accelerators, Nov.7-14, 1990, Hilton Head Island, So. Carolina, USA, Lecture Notes in Physics 400. *Frontiers of Particle Beams: Intensity Limitations* , Springer Verlag, pp.415-445.

[6] K. Yokoya, ABEL,'A Computer Simulation Code for the Beam-Beam Interaction in Linear Colliders', KEK-Report-85-9, Oct. 1985, also *Nucl. Instr. Meth.* **B251**, 1 (1986).

[7] C.J.S.Damerell, *Nucl. Instr. Meth.* **A342**, 78 (1994) and "Vertex Detectors at Linear Colliders(Present and Future), RAL Report, RAL-94-096.

[8] Private communication with C.J.S. Damerell.

[9] This detector might have about 1000 readout channels since 0.4cm^2 area of a CCD vertex detector can be read out at 150Hz as described in p83-86 of "JLC-I", KEK Report 92-16.